

SCIENTIFIC REPORTS



OPEN

Synchrony and asynchrony between an epigenetic clock and developmental timing

Akina Hoshino¹, Steve Horvath², Akshayalakshmi Sridhar¹, Alex Chitsazan³ & Thomas A. Reh¹

Epigenetic changes have been used to estimate chronological age across the lifespan, and some studies suggest that epigenetic “aging” clocks may already operate in developing tissue. To better understand the relationship between developmental stage and epigenetic age, we utilized the highly regular sequence of development found in the mammalian neural retina and a well-established epigenetic aging clock based on DNA methylation. Our results demonstrate that the epigenetic age of fetal retina is highly correlated with chronological age. We further establish that epigenetic aging progresses normally *in vitro*, suggesting that epigenetic aging is a property of individual tissues. This correlation is also retained in stem cell-derived retinal organoids, but is accelerated in individuals with Down syndrome, a progeroid-like condition. Overall, our results suggest that epigenetic aging begins as early as a few weeks post-conception, in fetal tissues, and the mechanisms underlying the phenomenon of epigenetic aging might be studied in developing organs.

Human and mouse studies have shown that DNA methylation-based biomarkers can provide a way to measure chronological age across the entire age spectrum and in all tissues, despite the fact that patterns of DNA methylation vary considerably across tissues^{1–4}. Remarkably, so-called DNA methylation epigenetic clocks provide highly accurate age estimators for individuals from 0 to 100 years old^{3,5,6}. The Horvath clock is based on the weighted average of 353 CpGs, whereby methylation of 193 CpGs is positively correlated with age, while methylation of the other 160 CpGs is negatively correlated with age⁷. This DNAm clock has also been used to investigate cases of epigenetic age acceleration, where the individual might be aging more rapidly than their chronological age. In particular, Horvath and colleagues have shown that the age-related phenotypes observed in some progeroid syndromes (e.g., Werner syndrome, Hutchinson Gilford Progeria Syndrome; Down syndrome) correlates with accelerated epigenetic aging^{8,9}. While many studies have thus validated the DNAm clock in many different tissues after birth, a recent study shows this clock might also apply prenatally. Analysis of DNA extracted from cord blood from neonates demonstrated that gestational age can be reliably predicted between 24 and 44 weeks¹⁰. These results are consistent with results from induced pluripotent stem cells (iPSCs) that show they are considerably younger than the cells they were derived from^{3,11}.

The studies described above thus motivated us to evaluate the range in human fetal development over which the Horvath’s epigenetic clock is applicable. The use of iPSCs in age-related disease modeling, show biomarkers of age-acceleration before the onset of age-related manifestations of the disease^{12–17}. Evidence from many labs for both mouse and human indicates that developmental timing is conserved in tissues derived *in vitro* from pluripotent stem cells, such as cerebral and retinal organoids^{18–22}, but it is not known whether tissues derived from iPSCs follow the same epigenetic clock as their corresponding fetal tissues.

To investigate the ability to estimate the age in embryonic or fetal tissue, we utilized the highly regular sequence of development found in the mammalian neural retina^{23,24}. During retinal development, the six main types of neurons are generated in a sequence that is largely conserved across vertebrates. Ganglion cells, horizontal cells, and cone photoreceptors are produced by progenitors early in retinogenesis, while most rod photoreceptors, amacrine cells, and bipolar cells are generated in the second half of the neurogenesis period^{23,24}. This well-defined sequence of cell generation in the vertebrate retinas is analogous to that which occurs in other developing neural

¹Department of Biological Structure, University of Washington, Seattle, WA, 98195, USA. ²Human Genetics and Biostatistics, David Geffen School of Medicine, University of California Los Angeles, Gonda Research Center, Los Angeles, CA, 90095-7088, USA. ³Department of Biochemistry, University of Washington, Seattle, WA, 98195, USA. Akina Hoshino, Steve Horvath and Akshayalakshmi Sridhar contributed equally. Correspondence and requests for materials should be addressed to T.R. (email: tomreh@uw.edu)

tissues, such as the *Drosophila* neuroblast lineage²⁵ and the cerebral cortical laminar-specification²⁶, and provides an excellent model system to study developmental timing. Thus, this study explores the link between developmental and chronological age using the human retina as a model. Our results show for the first time that (1) the epigenetic clock extends back to at least 8 weeks of gestational age, and possibly to conception, (2) the epigenetic clock continues to tick in explant cultures, thus providing potential to explore the mechanisms underlying DNAm epigenetic age, (3) that organoids derived from ESCs also show a correlation between their DNAm age and their chronological age from the onset of the differentiation protocol, and (4) the progeroid-like disorder, Down syndrome, leads to accelerated DNAm age in fetal stages, but does not cause dramatic correlated acceleration of developmental stage, suggesting that the epigenetic clock and the developmental clock are likely independent. Overall, this study provides both an independent way to measure developmental time and establishes the human retina as a potential experimental model to study epigenetic aging *in vitro*.

Results

During retinal development, retinal neurons are specified in a stepwise, temporally-restricted sequence. In the fetal human retina, the first wave of neurogenesis generates ganglion cells, cones and horizontal cells, resulting in a 3-layered retina by day 50 (Fig. 1A, FD50). By 90 days, the second wave of neurogenesis is initiated, leading to the birth of bipolar, amacrine, rod photoreceptors, and Müller glia (FD90). Following the generation of retinal cells, retinal circuits continue to mature (FD110+). We have previously described these main epochs of human fetal development using RNAseq (Hoshino *et al.*²⁷) and found approximately 3000 developmentally regulated genes organized into 6 superclusters that highlight meaningful gene expression patterns across the ages D52 to D136 (Fig. 1B).

We analyzed the DNA methylation patterns from the same developmental ages as the RNAseq study to evaluate DNA methylation patterns. These analyses utilized the Horvath epigenetic clock that estimates age based on the DNA methylation (DNAm) levels of 353 CpGs. The resulting age estimate is referred to as DNAm age, and is in units of years, and negative and positive values of epigenetic age correspond to prenatal samples and postnatal samples, respectively. Our data demonstrates that the epigenetic clock is indeed maintained in the retina, and we found a strong correlation ($r = 0.80$, $p < 0.0001$, Fig. 1C,C'; Supplemental Fig. 1) between the epigenetic age and chronological age in the fetal retina. This degree of correlation is typical of that which we observe in human adult tissues with the Horvath clock; however, we did not see a similar correlation with other types of DNAm clocks⁵ (Supplemental Fig. 2). The more rapid change in DNAm age in the fetal retinal samples (Fig. 1C red dots) and fetal cortical samples indicates that the epigenetic clock "ticks" more rapidly in the fetal samples than in mature tissues (Supplemental Fig. 1B). The steeper clock rate in the fetal samples allows for better resolution in developing tissues than what is possible in adult tissue, and as a result, one can detect differences in epigenetic age in a few weeks, as opposed to a few years in adult tissues.

To better understand the relationship between the epigenetic clock and the retinal developmental clock that controls the rate of neurogenesis and timing of gene expression, we relied on the developmental gradient present in the fetal retina. Within the human retina, there exists a central-to-periphery gradient, where the center (Central (C) or macula (M)) is developmentally accelerated by several weeks when compared with the periphery (P). RNAseq data (Hoshino *et al.*²⁷) demonstrates that the central retina turns off progenitor genes earlier than the periphery at the same age (Superclusters 1&2), and consecutively turns on differentiating photoreceptor cell markers faster (Supercluster 4) (Supplemental Fig. 3). This developmental gradient is particularly noticeable in the generation and morphology of later born cell types, as shown in a D96 retina (Fig. 1D). The peripheral retina at this stage is comprised of photoreceptors (RCVRN, magenta) in the outer layers, followed by progenitors (SOX2, cyan) and ganglion cell layer (ELAVL3/4, green). In comparison, the fovea is developmentally accelerated, as evidenced by the RCVRN positive cones that have a box-shape morphology and RCVRN-positive bipolar cells (dashed rectangle box). In addition to ganglion cells, the fovea also has a distinct population of amacrine cells in the INL (ELAVL3/4, green) and developing Müller glial cells (SOX2, cyan). Interestingly, comparisons of the epigenetic clock from different regions of the retina revealed no major differences; different parts of the retina followed the same trend as the whole retina and maintained their epigenetic age, even though central retina is developmentally accelerated compared to peripheral retinal regions (Fig. 1E). This result suggests that the developmental clock and the epigenetic clock might be controlled independently.

In order to test whether the epigenetic clock continues to progress when isolated from the rest of the organism, epigenetic clock analyses were performed on explant cultures of fetal retinas from various stages of development. Explants were maintained for 3 to 6 weeks and the rate of development and the epigenetic clock was evaluated by immunofluorescence/RNAseq, and DNA methylation respectively. Figure 2A shows examples of retinas that were either freshly harvested (*in vivo*) or maintained in explant culture for 3 weeks. With the exception of retinal ganglion cells, which do not survive well in explant cultures, other retinal cell types appear to differentiate in approximately normal numbers and with appropriate timing of the onset of many cell-type specific marker genes (Photoreceptors and bipolar cells marked by RCVRN/OTX2 expression in magenta/cyan respectively; Supplemental Fig. 4). More systematic evaluation of retinal development *in vitro* was possible with RNAseq (Fig. 2B–D). Using the superclusters that capture developmental progression in the human retina²⁷, and comparing *in vitro* and age-matched *in vivo* development samples, we observed that the explant cultures closely followed normal retinal development (Fig. 2B). Examples of key developmental genes, SFRP2 (an early progenitor gene, Fig. 2C, upper) and NRL (an early rod photoreceptor-specific marker, Fig. 2C, lower) show similar developmental timing between the explant cultures (pink symbols) and the *in vivo* retinas (green symbols for matched pair and gray symbols for all fetal retinal *in vivo*). Figure 2D shows boxplots for the top 100 genes in Supercluster 4, demonstrating developmental progression between retinal pairs when one was taken for RNAseq acutely and the other maintained *in vitro* for 3 weeks. In all cases, gene expression shows appropriate developmental progression *in vitro*.

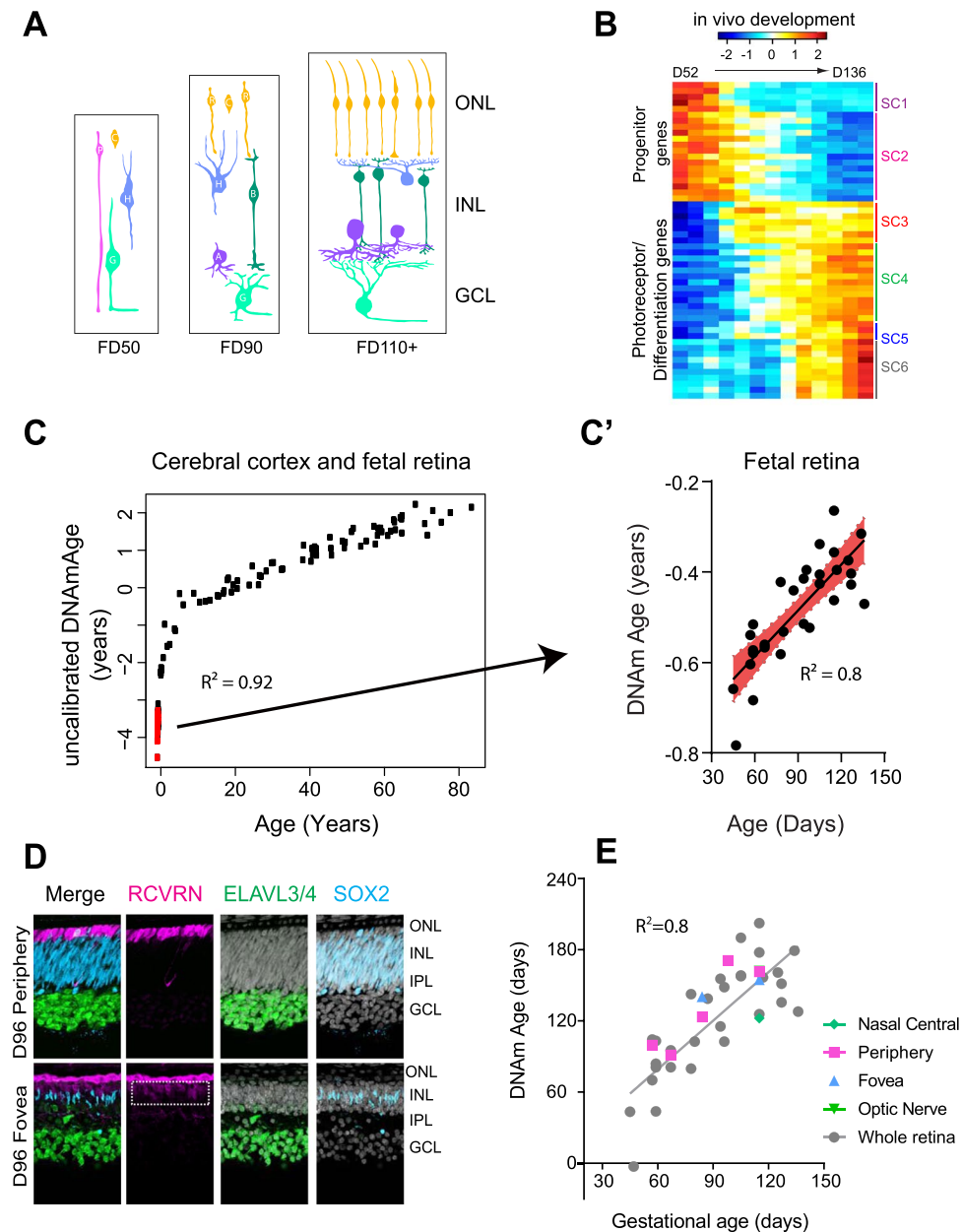


Figure 1. (A) Development of the retina proceeds in a regular order of cell addition, with the progenitors (P, pink) first making the early cell types, ganglion cells (G, green), the horizontal cells (H, blue), and then the cones (C, orange), followed by a later phase of histogenesis where the late cell types are generated, including the amacrine cells (A, purple), the rod photoreceptors (R, orange), the bipolar cells (B, dark green), and the Müller glia (not shown). Cell genesis is followed by a regular sequence of differentiation events during which the cells elaborate dendrites and make synapses with one another. (B) Bulk RNAseq of fetal retina was organized into six superclusters to highlight gene expression trends during retinogenesis (data re-plotted from Hoshino *et al.*²⁷). (C) Chronological age (x-axis) versus epigenetic age (y-axis) of cerebral cortex and fetal retina. C. Expanded view of the correlation between DNA mAge and gestational age of fetal retinal samples. Slope = 1.235 ± 0.1676 , R square = 0.8; NOTE: that the time axes are not the same between C and C'. (D) Human fetal retina exhibits characteristic central to periphery gradient, where the fovea is more accelerated than the periphery (P) at the same age. The periphery is mostly comprised of progenitors (SOX2, cyan), photoreceptors (RCVRN, magenta) and ganglion/early amacrine cells (ELAVL3/4, green) in a D96 fetal retina while fovea exhibits box-shaped cones and additional RCVRN-positive bipolars (dashed rectangle), amacrine (ELAVL3/4 in the INL) and Müller glia markers (SOX2 in INL) indicative of accelerated retinal development (DAPI in white). (E) Epigenetic age remains conserved across different regions of the retina, despite their developmental differences. (ONL = Outer nuclear layer, INL = Inner nuclear layer, GCL = Ganglion cell layer, IPL: Inner plexiform layer; SC = supercluster). $R^2 = 0.8$.

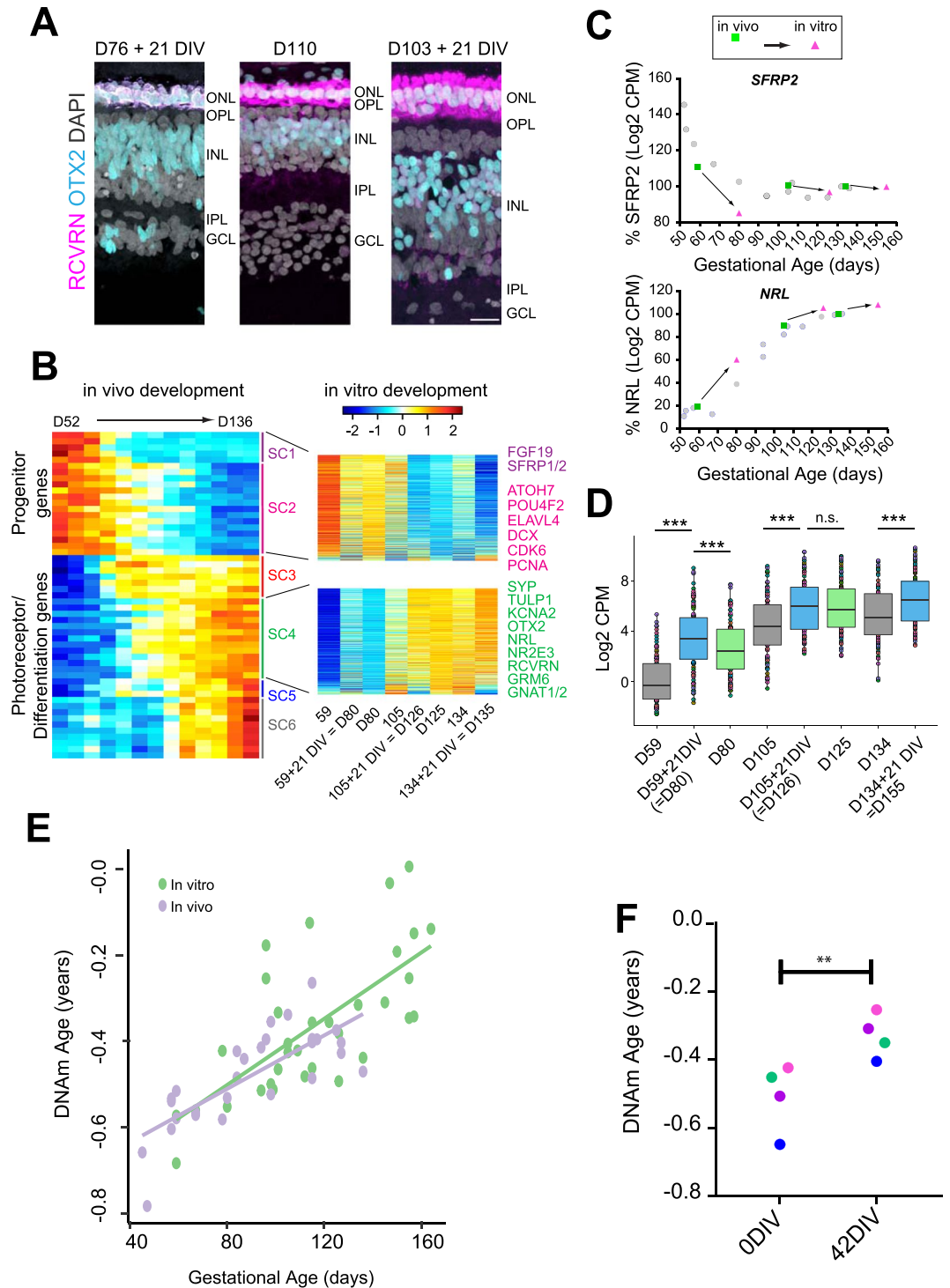


Figure 2. (A) D76 and D103 retinal explants maintained for 21 DIV were compared to a D110 fetal retina processed acutely; immunostaining with OTX2 (cyan) and RCVRN (magenta) to label photoreceptors and bipolar cells and DAPI (white, all cells). (B) (Left) Heatmap of RNAseq data of human retinas from D52 to D136 (from Hoshino *et al.*²⁷) showing all the Superclusters (SCs) of genes based on their developmental expression profiles. Heatmaps of SC1 and SC2 (top) and SC4 (bottom) gene expression of retinal pairs from D59, D105, and D134, with one retina taken for RNAseq immediately postmortem and the other after 21 days *in vitro*. (C) Plots for SFRP2 (a progenitor gene) and NRL (a rod photoreceptor gene) for each pair to show that the trends for the expression levels of these genes *in vitro* (pink symbols) is similar to that found in normal *in vivo* development (green symbols for paired retina, gray symbols for all other retinas). (D) Boxplot of expression level of the top highly expressed 100 genes from SC4 for the retinal pair data plotted in B, ($p < 0.0001$, two-sided paired t-test, NS = 0.9). (E) Retinas maintained *in vitro* for 42 days (blue) follow the same progression in epigenetic DNAm ages (y-axis) as those of uncultured retinas (gray dots). (F) Retinal pairs (matched colors), one analyzed immediately post-mortem and the other after 42 days *in vitro*, show that the epigenetic DNAm age (y-axis) continues to progress *in vitro* (p -value < 0.005 , one-sided paired t-test).

Given the fact that normal developmental timing is well conserved in human fetal retinal explants, we next determined if epigenetic clock continues to operate normally *in vitro*. For these studies, we cultured 10 retinas, and analysis of their DNAm age (Fig. 2E, blue) showed they progressed at approximately normal rates when compared with the acutely isolated samples (Fig. 2E, gray). We also obtained four pairs of retinas, each pair from a single fetus, and extracted DNA from one eye immediately and the other eye after it was maintained in explant culture for 6 weeks (Fig. 2F). For each pair, the epigenetic clock continued at the normal rate *in vitro*, advancing to the appropriate chronological age as that of a similarly aged *in vivo* retina (Fig. 2F, $p < 0.005$). These results indicate that the synchrony between the developmental and aging clock is maintained outside the body, and suggest that the aging clock is an independent property of the tissue.

To further test whether the aging clock is an independent property of the tissue, we asked if cells that develop completely *in vitro* would also follow the epigenetic clock, such as stem cell-derived retinal organoids. Over the last decade, several groups including ours, have demonstrated the ability of pluripotent stem cells to mimic specific stages of retinogenesis, and generate multilayered, stratified structures called retinal organoids^{16,18,28–30}. We derived retinal organoids from stem cells using the established protocols^{31,32} (Fig. 3A), and analyzed them for developmental and aging state. Similar to the fetal retina, ganglion cells are the earliest cell type expressed in the basal layers of organoid at 40 days (Fig. 3B,B; POU4F2 in green, higher PAX6 expression in magenta). Ganglion cells exhibited a ring-like organization within the basal layers of the organoids, and expressed markers for POU4F2 and ELAVL3/4. Following ganglion cell expression, cone photoreceptors were the next cell type to develop in the outer layers of organoids (Fig. 3D–F, OTX2, magenta). Multiple layers of photoreceptors were visible by Day 80, and further differentiation yielded early rod photoreceptors (Fig. 3F, NR2E3 in cyan— looks white in figure because of overlap.) Organoids approximately follow the developmental clock of the fetal retina; however, it is difficult to exactly compare them with a resolution of less than 3 weeks, since there is a large central-to-peripheral developmental gradient across the retina and it is not clear what the retinal position the organoids represent. Moreover, the cellular composition of the organoids is not exactly the same as the fetal retina, since ganglion cells do not survive well *in vitro*. Nevertheless, RNAseq cluster analysis of organoids from Day 20 to Day 90 shows that expression of Supercluster 1&2 genes decreased while expression of Supercluster 4 genes increased with time (Fig. 3G).

Following RNAseq analyses, DNA from the same samples was utilized for epigenetic clock analyses. We found that the DNAm age of the retinal organoids increased with age since the onset of differentiation (Fig. 3H). Interestingly, the epigenetic clock is somewhat accelerated in organoids. For example, samples from 60–100 days of differentiation had a DNAm age comparable to nearly one year old postnatal tissue samples. Nevertheless, their DNAm age remained highly correlated with chronological age after their exit from the pluripotent stage.

So far, our data demonstrates that the epigenetic clock of fetal retinal tissue is usually synchronized with development age. Previous analyses have demonstrated accelerated aging in Down syndrome, from both clinical manifestations and the epigenetic methylation clock. Using blood leukocytes, whole blood, and post-mortem brain regions, Horvath *et al.* 2015 reported a highly significant age acceleration of 4–11 years in the Down syndrome cases³³. Given that the epigenetic age can already be measured in fetal retinal samples, we asked whether epigenetic clock acceleration in Down syndrome might already be measurable in fetal development. We measured the epigenetic age in four Trisomy 21 samples and one Trisomy 13 sample, and we found a significant age acceleration in the four Trisomy 21 samples, but not the Trisomy 13 sample (Fig. 4A, $p < 0.0001$). Interestingly, the acceleration of the epigenetic clock in these samples was not accompanied by an acceleration of their developmental clock: immunofluorescent labeling of retinal sections show similar patterns of cell differentiation in the Down syndrome cases as in the age-matched normal fetal retinas (Fig. 4B). These images show comparisons between Down syndrome and normal fetal retinas for photoreceptors (RCVRN, OTX2) and bipolar cells (VSX2) amacrine cells (ELAVL3/4) and synapses (VGLUT/SLC17A7). If there was accelerated development in the Down syndrome retinas, we would expect to see a greater number of VSX2+ bipolar cells, more mature photoreceptors (RCVRN) and an increase in VGLUT/SLC17A7 labeling, but we do not see these changes. We further analyzed the developmental state of the Down syndrome retinas using RNAseq (Fig. 4C,D), and our analysis shows similar patterns of gene expression in the ~3000 supercluster genes between Down syndrome and normal retinas (Fig. 4C, Supplemental Fig. 5B–D). The heatmaps shown that the overall trends in the Down syndrome samples follow those of the normal fetal retinas (Fig. 4C); however, there are some differences, and the MA plot (Fig. 4D) shows that 95 of the supercluster genes show significant differences (3% of total supercluster genes; Extended Data Table 3). Of these 95 genes, 8 were on Chr21 and these all were increased in the Down syndrome samples (Supplemental Fig. 5A and Extended Data Table 3).

Discussion

In the past five years a number of reports have shown that distinct epigenetic changes occur during the process of aging, and these changes show a high degree of correlation with chronological age^{4,34,35}. The pan tissue clock by Horvath (2013) accurately estimates age in children^{3,4}, and is applicable to DNA from all tissues and nucleated cells, with widely varying cellular composition, from birth to old age. Although most of the previous studies that have shown a high degree of correlation between DNAm age and chronological age have been in mature tissues, two previous studies have shown that the same aging clock might also apply to developing tissues^{10,36}. In this report, we have confirmed these earlier studies that used cord blood in neonates and fetal brain, extending this correlation to fetal retinal tissues as well. We also find that the resolution of the clock in fetal tissue is much better than in the adult tissues, like the earlier report in fetal brain. Differences in tissue age of just 4–6 weeks can be discriminated by the epigenetic clock in fetal tissue, while adult tissue can only be discriminated with this clock within 2–4 years. Interestingly, the epigenetic clock resolution is intermediate in infants and children, consistent with a general slowing in the clock rate with maturation. Thus, together with these previous reports, it appears that the epigenetic clock age operates across lifespan, including fetal stages of human development.

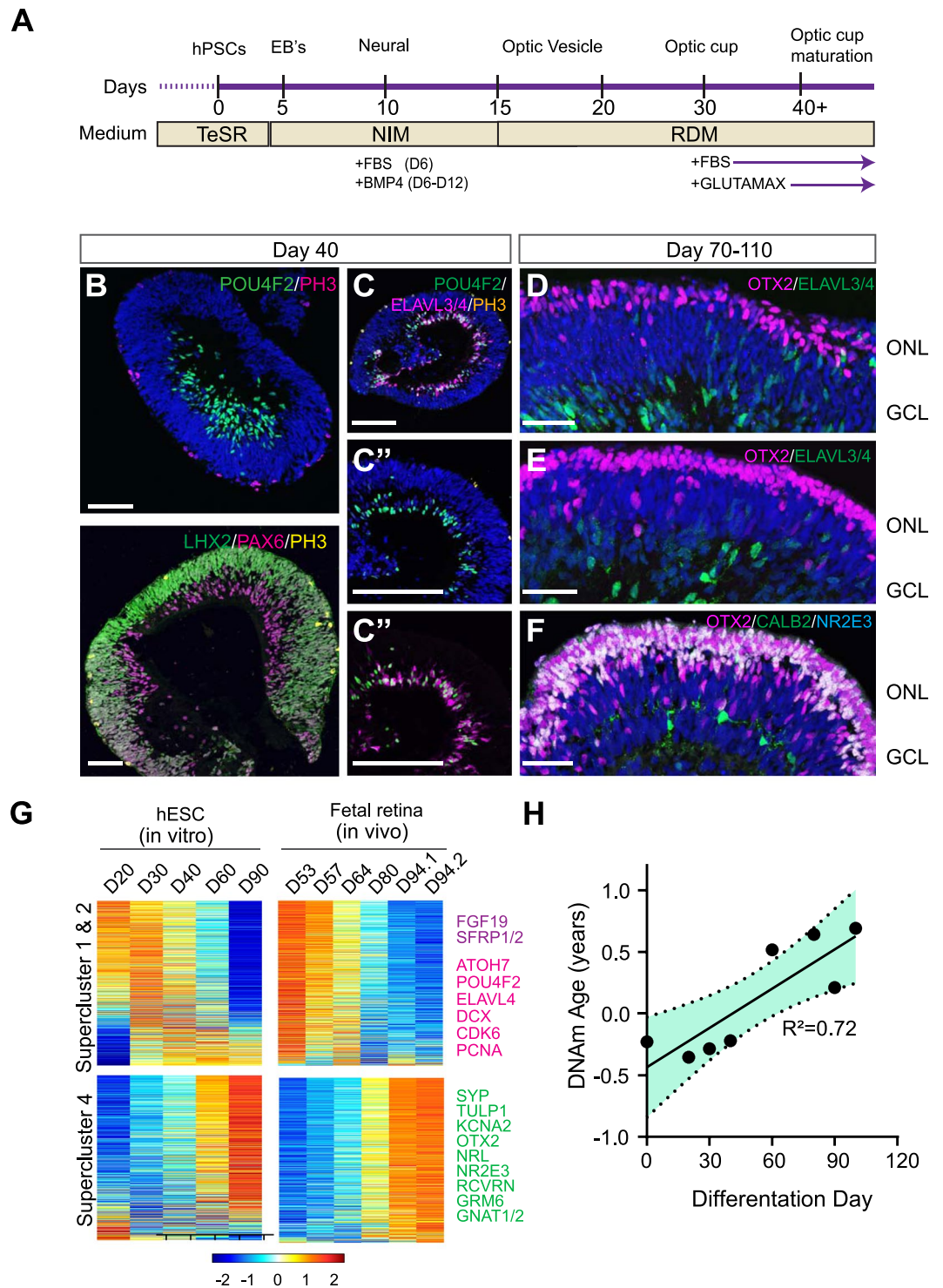


Figure 3. (A) hPSCs were directed to generate retinal organoids in a step wise manner as previously described^{31,32,55,57}. (B,C). By 40 days, ganglion cells were readily identified by the expression of POU4F2 and PAX6 within inner layers of organoids, and remained distinct from retinal progenitors (LHX2). Early organoids expressed ELAVL3/4 and POU4F2 in a ring-like manner within basal layers of organoids, (C, 200 μ m, C'-C'' 50 μ m), while mitotic marker PH3 was localized towards the apical surface of organoids. (D-F). By 70 days, OTX2 positive photoreceptors were seen toward the apical surface of organoids (D), and became increasingly abundant by Day 80 (E). By 110 days, multiple layers of photoreceptors were visible on the apical surface, and further differentiation yielded NR2E3 positive rod photoreceptors (F). (G) Bulk RNAseq analysis demonstrate that organoids mimic fetal retina gene expression patterns at comparative stages. Supercluster 1 and 2 genes marking retinal progenitor, cell cycle, and ganglion cells genes decrease in expression while supercluster 4 genes indicative of later-born retinal cell types increase expression at later timepoints. (H) DNAm (years) age plotted against the day since the differentiation was initiated (in days) ($p < 0.0073$).

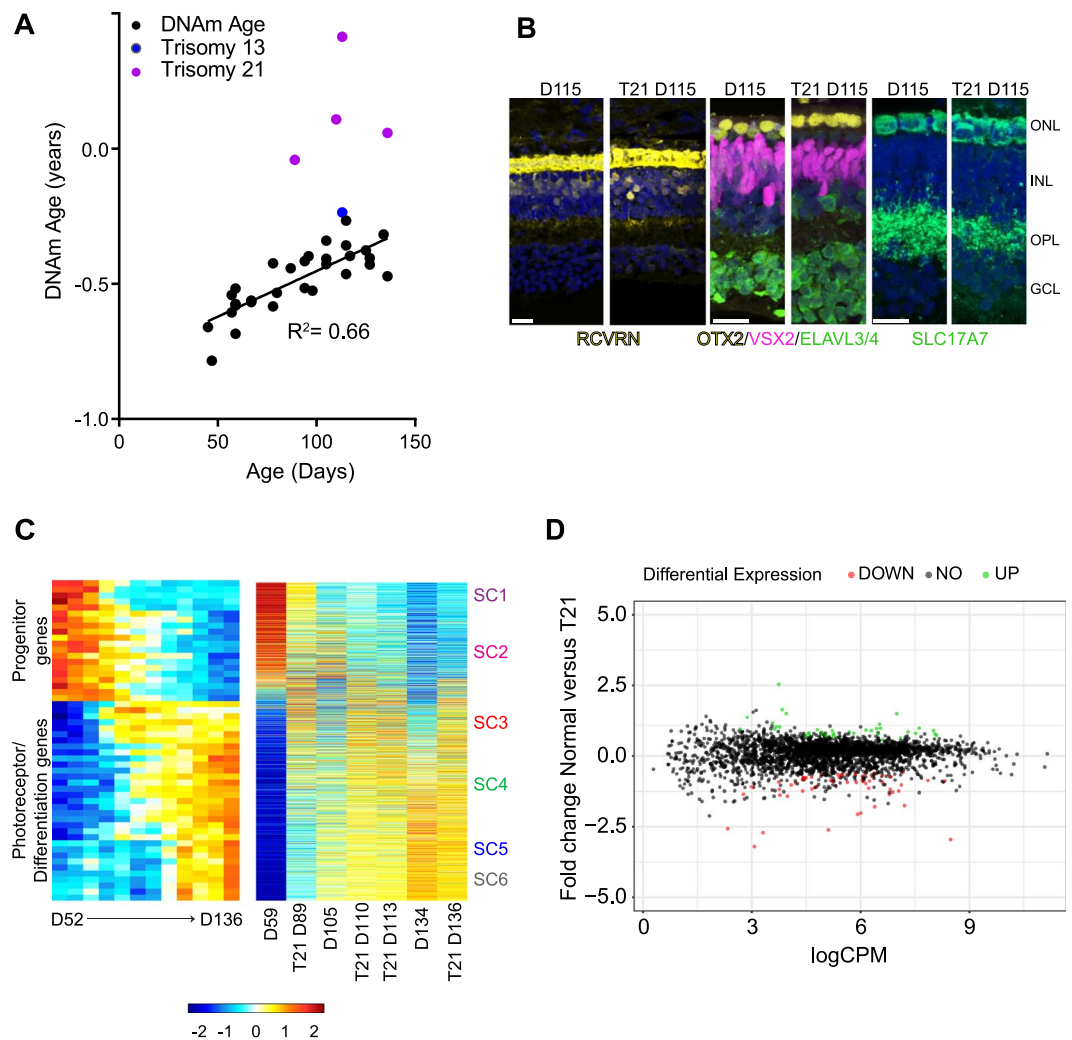


Figure 4. (A) DNAm age (years) plotted against chronological age for Trisomy 21 (T21, Down syndrome, magenta) and Trisomy 13 (blue). The T21 retinas were significantly accelerated when compared to the normal fetal retina (p value < 0.0001) (B) Immunostaining of Down syndrome and normal fetal retinas for photoreceptors (RCVRN, OTX2) and bipolar cells (VSX2) amacrine cells (ELAVL3/4) and synapses (VGLUT1/SLC17A7) taken from D115 age-matched samples at equivalent eccentricity (scale = 20 μ m). (C) Heatmaps showing bulk RNAseq of Down syndrome and normal fetal retinas (right) compared with supercluster genes from Hoshino *et al.*²⁷ (left). D. MA plot showing the similarity of gene expression between WT and Trisomy RNAseq with all ages combined and significantly (p < 0.05) upregulated genes (green) and significantly (p < 0.05) downregulated genes (red).

Having established that the epigenetic clock can be used to study age in developing tissue, we went on to study the relationship between the epigenetic and the developmental clock that controls the sequence and relative time of events in developing tissues. We have found that the epigenetic clock continues to advance in explant cultures of fetal retina and shows a similar relationship with developmental stage and chronological age in organoids derived from pluripotent stem cells. However, we also find that the developmental clock and the epigenetic clock are not always in synchrony: (1) developmental gradients across the retina are not reflected in DNAm age, (2) organoids are significantly accelerated in DNAm age, despite their similar developmental time with fetal retinas, and (3) the epigenetic clock is significantly accelerated in fetal retina from Down syndrome samples, though the developmental clock does not show major changes and remains correlated with gestational age.

An interesting feature of the epigenetic clock is that it is not restricted to a specific tissue. Previous studies have shown that this is a tissue independent correlation, with a similar age estimate from the same CpGs regardless of tissue type, including brain, skin, kidney, colon, lung, etc.⁷. Our study extends this correlation to the neural retina, and further supports the hypothesis that the age is present in all cell types within the tissue. The range of ages of retinal development included in this study encompass major changes in cellular composition; in the early fetal stages, the retina is primarily composed of retinal progenitors and ganglion cells, while at the later time points in our study, the retina is largely composed of amacrine cells and photoreceptors (Fig. 1A). Nevertheless, the epigenetic clock appears to be not dependent on the relative percentages of the different cell types. Additionally,

the retina shows major stage-dependent changes in the DNA methylation status of CpGs at the promoters of differentially expressed gene promoters³⁷, like other developing tissues, but the DNAm age does not depend on whether the 353 CpGs are in gene promoters of genes expressed in the tissue. Fewer than 10% of the 353 CpGs that comprise the epigenetic clock are in promoters of genes differentially expressed in developing retina³⁷. This is similar to fetal brain³⁸, where large changes in the methylome accompany a similar range of fetal developmental stages, but the 353 CpGs of the epigenetic clock correlate with gestational age rather than with tissue composition or developmental gene expression. Thus, the developmental changes in methylation occur in parallel with the epigenetic clock, and appear to be reflected in all cells, even transient progenitor populations.

Despite the strong correlation with gestational age and DNAm age in the fetal samples, the epigenetic clock and the developmental clock are not always in synchrony. The development of mammals shows a tight correlation between the gestational age and developmental stage, and staging fetal and embryonic tissues depends on this correlation. However, we took advantage of the natural developmental gradient in the retina to explore the degree of synchrony between the developmental clock and the epigenetic clock. In the human retina there is a pronounced central-to-peripheral gradient in the relative timing of developmental events. For example, the onset of rhodopsin expression in rod photoreceptor in central retina occurs at FD105, but not until FD 250–280 in the far periphery, a difference of over 4 months³⁹. The epigenetic clock, however, shows that the central and peripheral regions of the retina have a similar DNAm age, despite this difference in developmental stage (Fig. 1E). This result suggests that the DNAm age is a large-scale property of the tissue, unaffected by regional differences in developmental timing within the tissue. A second example of disconnect between the epigenetic and developmental clock is shown by the analysis of the Down syndrome fetal retinas (Fig. 4). These retinas are significantly older by the DNAm age than their counterpart control retinas, by nearly a 3-fold change. However, this epigenetic clock acceleration does not cause a major change in the developmental clock. We saw few differences in the expression of the 3000 supercluster genes that encompass the major developmental epochs in human retina²⁷, between the Down syndrome retinas and age-matched control samples. Taken together, these results suggest that even though the DNAm aging clock and the developmental stage typically correlate with the gestational age, these clocks can be decoupled in some cases and likely represent two independent timing mechanisms.

Another interesting feature of the epigenetic clock revealed by our experiments is that this clock continues to correlate with gestational age *in vitro*. Previous studies in our lab and other have shown that fetal retinas can be maintained as explants *in vitro* for weeks, and that they continue to follow their normal course of development⁴⁰. In this study, we analyzed retinal explant cultures and found that in addition to following their normal developmental clock, they also advance in DNAm age at the same rate as they would have *in vivo*. To our knowledge, this is the first demonstration of an epigenetic aging clock continuing to tick *in vitro* and suggests that the clock depends on a fundamental process in the cells that is not altered by the artificial environment of the organ culture. Moreover, the mechanisms driving the Horvath epigenetic clock appear to be a property of cells and tissues, rather than the organism as a whole. Consistent with the fetal tissue explant results, we also find that the epigenetic clock tracks with *in vitro* age in pluripotent stem cell-derived tissues. Stem cell-derived organoids not only recapitulated the normal developmental timing, gene expression, and organization of the fetal retina, but also progressed in the DNAm age as a function of the time from the initiation of the differentiation protocol. Interestingly, the clock seemed slightly accelerated at later stages of development compared with the age-matched fetal samples, but it still remained highly correlated with developmental age. A previous report by Horvath demonstrated that the process of generating iPSC cells resets the epigenetic clock, and undifferentiated cells are significantly younger than postnatal and adult tissues⁷. While DNAm age of stem cells is negative as expected, stem cells exhibit a range of ages, between -0.2 to -0.5 years, depending on passage number and effects of different culture condition (with or feeders). The relative acceleration of the stem cell-derived retinal organoids in our experiments might therefore reflect an incomplete initial reset of the epigenetic clock in pluripotent stem cells.

Our results also have several implications for stem cell biology and disease modeling. Our data demonstrates that the epigenetic clock is a reliable and quantitative determinant of gestational age and developmental stage at fetal stages of human development, and can serve as a biomarker of accelerated aging in a progeroid syndrome⁸. Although iPSC-derived *in vitro* models of age-related diseases can sometimes demonstrate phenotypic changes related to the disease *in vitro*^{14,15,41}, this often requires the cultures be stressed. The fact that the epigenetic clock tracks normal aging as early as fetal stages in a manner that is essentially equivalent to age-matched organoids, provides a biomarker for age-related diseases that may not require the manifestation of the age-related phenotype. Moreover, analyses of samples with Down syndrome show the pronounced acceleration of the DNAm age even in fetal stages, similar to what has been observed in adult tissues³³. These findings support the conclusion that this biomarker of aging can be used from conception throughout the lifespan, for both normal and pathological aging. Our results also suggest that the mechanisms underlying the epigenetic clock (and aging more generally) might also be productively studied during development using *in vitro* cultures, either in organoids or explant cultures of fetal tissue.

Materials and Methods

All methods were performed following NIH and University of Washington guidelines and regulations.

Retinal explant cultures. Human fetal retinas with no identifiers were obtained from the Birth Defects Research Laboratory under an approved protocol (UW5R24HD000836) through the University of Washington. For whole retina RNAseq and DNA methylation studies, retinas were dissected and stored in Triol (Invitrogen, Carlsbad, CA) at -80°C . For immunohistochemistry, whole eyes were fixed in 4% paraformaldehyde for 1 hr at room temperature, cryoprotected in a sucrose gradient, and frozen in OCT (Sakura Finetek, Torrance, CA). Gender was determined by either anatomic identification or PCR. Age was estimated by a combination of clinical intakes, gestational ultrasound, crown-rump, and fetal foot length^{42,43}.

Retinas were dissected at the indicated ages and explanted onto 0.4 μm tissue culture inserts (Millipore, Billerica, MA). For the transcriptome and methylation studies, pairs of retinas were dissected and one was homogenized in Trizol immediately while the other eye was explanted and maintained in Retinal media (DMEM/F12 with GlutaMAX media containing 1% N2, 2% B27, 1% FBS, 1% PenStrep, 1x NEAA, 1x NaPyr, HEPES, and BDNF). For RNAseq studies, retinal explants were collected after 21 days in culture, and for DNA methylation assays, retinal explants were maintained for 42 days. For immunohistochemistry, unpaired retinas were cultured for 21 days.

Immunofluorescence and microscopy. 20 μm serial sections of cryoembedded retinas were first blocked in blocking buffer (10% normal horse serum in 0.5% Triton-X100/PBS) for 1 hour at room temperature and then incubated in primary antibodies diluted in blocking buffer overnight at 4C. The following day, retinas were washed 5 times in PBS, incubated with the appropriate 488/568/647 fluorophore-conjugated secondary antibodies and DAPI for 1 hour at room temperature. Samples were washed again before cover slipping using Fluoromount-G (SouthernBiotech, Birmingham, AL). Details of the antibodies used in this study are provided in Extended Data Table 2.

Whole retina RNAseq. Total RNA from acutely collected or cultured whole retinal pairs (D59, D105, and D134) were extracted according to manufacturer's instructions. RNA integrity was assessed using the Agilent 4200 TapeStation (Agilent Technologies, Santa Clara, CA) and quantified with Trinean DropSense Spectrophotometer (PerkinElmer). RNAseq libraries were generated using the TruSeq RNA Sample Prep kit (Illumina) and 50 base pair paired-end sequencing was performed using an Illumina HiSeq. 2500. Intersection-strict (<https://htseq.readthedocs.io/en/master/count.html>).

DNA extraction and sample preparation for DNA methylation. Genomic DNA of the retinas was precipitated from the interphase and phenol phase of the TRIzol solution using 100% ethanol. The DNA pellet was washed 3 times with 0.1 M sodium citrate/10% ethanol solution and once with 75% ethanol. The pellet was then resuspended in 8 mM NaOH buffer or concentrated using gDNA Clean and Concentrator kit (Zymo Research, Irvine, CA). Concentration of gDNA was measured using the Nanodrop. Bisulfite conversion was performed on 500 ng of DNA using the Illumina Infinium Methylation Assay protocol in the EZ DNA Methylation kit (Zymo Research). Following the desulphonation and wash steps, converted DNA was eluted in 12 μl of the M-Elution buffer and then loaded onto the Infinium Human Methylation 450K BeadChip kit (Illumina, #WG-314-1003) or Infinium Methylation EPIC BeadChip kit (Illumina, #WG-317-1002). Methylation dataset of the cerebral cortex was previously published⁴⁴.

Epigenetic clock analysis. The standard protocol of Illumina methylation assays quantifies methylation levels by the β value using the ratio of intensities between methylated (signal A) and un-methylated (signal B) alleles. Thus, β values range from 0 (completely un-methylated) to (completely methylated)^{45,46}. We used the “noob” normalization method implemented in the “minfi” R package^{47,48}, but our findings remain qualitatively the same for all other normalization methods implemented in the “minfi” package. A vast body of literature has demonstrated that chronological age has a profound effect on DNAm levels^{49–53}. Recent studies demonstrate that DNAm levels give rise to accurate estimators of age^{3,5,54}. Unlike previous age estimators that apply to saliva or blood, the pan tissue DNAm age estimator, based on 353 CpGs, is broadly applicable to all human nucleated cells, tissues, and organs. The pan tissue age estimator is defined as a prediction method of age based on the DNAm levels of 353 CpGs. The predicted age, referred to as epigenetic age or DNAm age, is in units of years. Negative DNAm age estimates indicate prenatal samples whereas positive DNAm age estimates correspond to postnatal samples. DNAm age correlates with chronological age (at the time of sample collection) in sorted cell types (glial cells, neurons, CD4+ T cells, monocytes, B cells) and tissues and organs including whole blood, brain, breast, kidney, liver, lung, and saliva⁷. The epigenetic clock (and software) applies to data generated using all Illumina array platforms (Infinium 27K, 450K, and EPIC). Mathematical details and software tutorials for the epigenetic clock can be found in the Additional files of Horvath, 2013⁷.

Whole retina RNAseq data analysis. RNAseq data from developing human (D59–D136) retinas were generated previously²⁷. Differentially expressed genes from the human dataset were reclustered using affinity propagation clustering, using the R package *apcluster* (v.1.4.4) and *corSimMat* argument. The supercluster designation (SC1–6) of a gene is the same as previously described²⁷. Trisomy 21 retinas and retinal organoids (Day20–Day90) were sequenced at Fred Hutch Cancer Research Center. The quality of the FASTQ files was evaluated using FastQC (<https://www.bioinformatics.babraham.ac.uk/projects/fastqc/>) and reads that didn't pass Illumina's base call quality threshold were removed. We used HISAT v2.1.0 (<https://ccb.jhu.edu/software/hisat2/index.shtml>) to align reads to the hg38 reference, then counts were called using HTseq-count v0.6.0 using intersection-strict (<https://htseq.readthedocs.io/en/master/count.html>). Genes that had 0 counts across all samples were removed, and a table of normalized, log₂-transformed counts per million (CPM) values were generated using edgeR (v.3.18.1).

Stem cell culture. hPSCs were maintained and differentiated as described previously^{16,30,32,55,56}. Briefly, cell lines H1 and H9 (WiCell, ISCRM core) were maintained in Matrigel (BD Biosciences) and mTeSR1 (Stemcell technologies) medium. Differentiation was initiated by passaging with dispase and the resultant embryoid bodies were transitioned to a 1:1 combination of TeSR and Neural induction medium (NIM; DMEM/F12, N2 supplement, MEM non-essential amino acids, Pen Strep and heparin (2 $\mu\text{g}/\text{ml}$)) for 2 days, followed by complete NIM by Day 3 onwards. On day 5, BMP4 (0.05 $\mu\text{g}/\mu\text{L}$, R&D systems) was added to the EBs and these were subsequently plated with 10% FBS on day 8, followed by half-medium changes every other day up to Day 12. Optic-vesicle like

areas were morphologically identified by Day 20 and were manually dissected with a 30G needle attached to a 1ml syringe. These aggregates assembled into 3D spheres termed retinal organoids, and were maintained in Retinal differentiation medium (RDM; DMEM/F12, B27, MEM non-essential amino acids and Pen Strep) with 5% FBS and 2 mM Glutamax (Gibco) for long-term cultures.

Statistics. All statistics were performed on GraphPad Prism 7/8 or in R (version 3.5.1). Two-sided paired t-tests were performed to test the differences of SC4 genes before and after culturing (Fig. 2D). ANOVA was used to calculate the slopes and the p-values for the explant cultures (Fig. 2E). For all other tests, one-sided paired t-test was performed. t-tests were significant if $P < 0.05$.

Data Availability

Whole retina RNAseq and DNA methylation array data will be deposited in the SRA (NCBI) and Gene Expression Omnibus.

References

- Bollati, V. *et al.* Decline in genomic DNA methylation through aging in a cohort of elderly subjects. *Mechanisms of ageing and development* **130**, 234–239, <https://doi.org/10.1016/j.mad.2008.12.003> (2009).
- Lim, U. & Song, M. A. DNA Methylation as a Biomarker of Aging in Epidemiologic Studies. *Methods in molecular biology (Clifton, N.J.)* **1856**, 219–231, https://doi.org/10.1007/978-1-4939-8751-1_12 (2018).
- Horvath, S. DNA methylation age of human tissues and cell types. *Genome Biol* **14**, <https://doi.org/10.1186/10.1186/gb-2013-14-10-r115> (2013).
- Horvath, S. & Raj, K. DNA methylation-based biomarkers and the epigenetic clock theory of ageing. *Nature reviews. Genetics* **19**, 371–384, <https://doi.org/10.1038/s41576-018-0004-3> (2018).
- Hannum, G. *et al.* Genome-wide methylation profiles reveal quantitative views of human aging rates. *Mol Cell* **49**, 359–367, <https://doi.org/10.1016/j.molcel.2012.10.016> (2013).
- Levine, M. E. *et al.* An epigenetic biomarker of aging for lifespan and healthspan. *Ageing* **10**, 573–591, <https://doi.org/10.18632/aging.101414> (2018).
- Horvath, S. DNA methylation age of human tissues and cell types. *Genome Biol* **14**, R115, <https://doi.org/10.1186/gb-2013-14-10-r115> (2013).
- Horvath, S. *et al.* Epigenetic clock for skin and blood cells applied to Hutchinson Gilford Progeria Syndrome and *ex vivo* studies. *Ageing* **10**, 1758–1775, <https://doi.org/10.18632/aging.101508> (2018).
- Maierhofer, A. *et al.* Accelerated epigenetic aging in Werner syndrome. *Ageing* **9**, 1143–1152, <https://doi.org/10.18632/aging.101217> (2017).
- Knight, A. K. *et al.* An epigenetic clock for gestational age at birth based on blood methylation data. *Genome Biol* **17**, 206, <https://doi.org/10.1186/s13059-016-1068-z> (2016).
- Vangeel, E. B. *et al.* Newborn genome-wide DNA methylation in association with pregnancy anxiety reveals a potential role for GABBR1. *Clinical epigenetics* **9**, 107, <https://doi.org/10.1186/s13148-017-0408-5> (2017).
- Chen, H. *et al.* Modeling ALS with iPSCs reveals that mutant SOD1 misregulates neurofilament balance in motor neurons. *Cell stem cell* **14**, 796–809, <https://doi.org/10.1016/j.stem.2014.02.004> (2014).
- Imaizumi, Y. *et al.* Mitochondrial dysfunction associated with increased oxidative stress and alpha-synuclein accumulation in PARK2 iPSC-derived neurons and postmortem brain tissue. *Molecular brain* **5**, 35, <https://doi.org/10.1186/1756-6606-5-35> (2012).
- Sances, S. *et al.* Modeling ALS with motor neurons derived from human induced pluripotent stem cells. *Nature neuroscience* **19**, 542–553, <https://doi.org/10.1038/nn.4273> (2016).
- Singh, R. *et al.* iPSC cell modeling of Best disease: insights into the pathophysiology of an inherited macular degeneration. *Hum Mol Genet* **22**, 593–607, <https://doi.org/10.1093/hmg/dds469> (2013).
- Meyer, J. S. *et al.* Optic vesicle-like structures derived from human pluripotent stem cells facilitate a customized approach to retinal disease treatment. *Stem Cells* **29**, 1206–1218, <https://doi.org/10.1002/stem.674> (2011).
- Ohlemacher, S. K. *et al.* Stepwise Differentiation of Retinal Ganglion Cells from Human Pluripotent Stem Cells Enables Analysis of Glaucomatous Neurodegeneration. *Stem Cells* **34**, 1553–1562, <https://doi.org/10.1002/stem.2356> (2016).
- Nakano, T. *et al.* Self-formation of optic cups and storable stratified neural retina from human ESCs. *Cell stem cell* **10**, 771–785, <https://doi.org/10.1016/j.stem.2012.05.009> (2012).
- Osakada, F. *et al.* *In vitro* differentiation of retinal cells from human pluripotent stem cells by small-molecule induction. *J Cell Sci* **122**, 3169–3179, <https://doi.org/10.1242/jcs.050393> (2009).
- Eiraku, M. *et al.* Self-organizing optic-cup morphogenesis in three-dimensional culture. *Nature* **472**, 51–56, <https://doi.org/10.1038/nature09941> (2011).
- Lamba, D. A., Karl, M. O., Ware, C. B. & Reh, T. A. Efficient generation of retinal progenitor cells from human embryonic stem cells. *Proc Natl Acad Sci USA* **103**, 12769–12774, <https://doi.org/10.1073/pnas.0601990103> (2006).
- La Torre, A., Hoshino, A., Cavanaugh, C., Ware, C. B. & Reh, T. A. The GIPC1-Akt1 Pathway Is Required for the Specification of the Eye Field in Mouse Embryonic Stem Cells. *Stem Cells* **33**, 2674–2685, <https://doi.org/10.1002/stem.2062> (2015).
- Livesey, F. J. & Cepko, C. L. Vertebrate neural cell-fate determination: lessons from the retina. *Nature reviews. Neuroscience* **2**, 109–118, <https://doi.org/10.1038/35053522> (2001).
- Reh, T. A. & Cagan, R. L. Intrinsic and extrinsic signals in the developing vertebrate and fly eyes: viewing vertebrate and invertebrate eyes in the same light. *Perspectives on developmental neurobiology* **2**, 183–190 (1994).
- Kohwi, M., Lupton, J. R., Lai, S. L., Miller, M. R. & Doe, C. Q. Developmentally regulated subnuclear genome reorganization restricts neural progenitor competence in *Drosophila*. *Cell* **152**, 97–108, <https://doi.org/10.1016/j.cell.2012.11.049> (2013).
- Molyneaux, B. J., Arlotta, P., Menezes, J. R. & Macklis, J. D. Neuronal subtype specification in the cerebral cortex. *Nature reviews. Neuroscience* **8**, 427–437, <https://doi.org/10.1038/nrn2151> (2007).
- Hoshino, A. *et al.* Molecular Anatomy of the Developing Human Retina. *Dev Cell* **43**, 763–779 e764, <https://doi.org/10.1016/j.devcel.2017.10.029> (2017).
- Phillips, M. J. *et al.* Blood-derived human iPSC cells generate optic vesicle-like structures with the capacity to form retinal laminae and develop synapses. *Invest Ophthalmol Vis Sci* **53**, 2007–2019, <https://doi.org/10.1167/iov.11-9313> (2012).
- Wahlin, K. J. *et al.* Photoreceptor Outer Segment-like Structures in Long-Term 3D Retinas from Human Pluripotent Stem Cells. *Sci Rep* **7**, 766, <https://doi.org/10.1038/s41598-017-00774-9> (2017).
- Zhong, X. *et al.* Generation of three-dimensional retinal tissue with functional photoreceptors from human iPSCs. *Nat Commun* **5**, 4047, <https://doi.org/10.1038/ncomms5047> (2014).
- Fligor, C. M. *et al.* Three-Dimensional Retinal Organoids Facilitate the Investigation of Retinal Ganglion Cell Development, Organization and Neurite Outgrowth from Human Pluripotent Stem Cells. *Sci Rep* **8**, 14520, <https://doi.org/10.1038/s41598-018-32871-8> (2018).

32. Sridhar, A., Ohlemacher, S. K., Langer, K. B. & Meyer, J. S. Robust Differentiation of mRNA-Reprogrammed Human Induced Pluripotent Stem Cells Toward a Retinal Lineage. *Stem Cells Transl Med* **5**, 417–426, <https://doi.org/10.5966/sctm.2015-0093> (2016).
33. Horvath, S. *et al.* Accelerated epigenetic aging in Down syndrome. *Aging Cell* **14**, 491–495, <https://doi.org/10.1111/accel.12325> (2015).
34. Freire-Aradas, A. *et al.* Tracking age-correlated DNA methylation markers in the young. *Forensic science international. Genetics* **36**, 50–59, <https://doi.org/10.1016/j.fsigen.2018.06.011> (2018).
35. Freire-Aradas, A. *et al.* Development of a methylation marker set for forensic age estimation using analysis of public methylation data and the Agena Bioscience EpiTYPER system. *Forensic science international. Genetics* **24**, 65–74, <https://doi.org/10.1016/j.fsigen.2016.06.005> (2016).
36. Spiers, H., Hannon, E., Schalkwyk, L. C., Bray, N. J. & Mill, J. 5-hydroxymethylcytosine is highly dynamic across human fetal brain development. *BMC genomics* **18**, 738, <https://doi.org/10.1186/s12864-017-4091-x> (2017).
37. Aldiri, I. *et al.* The Dynamic Epigenetic Landscape of the Retina During Development, Reprogramming, and Tumorigenesis. *Neuron* **94**, 550–568.e510, <https://doi.org/10.1016/j.neuron.2017.04.022> (2017).
38. Spiers, H. *et al.* Methylomic trajectories across human fetal brain development. *Genome Res* **25**, 338–352, <https://doi.org/10.1101/gr.180273.114> (2015).
39. Hendrickson, A. *et al.* Rod photoreceptor differentiation in fetal and infant human retina. *Experimental eye research* **87**, 415–426, <https://doi.org/10.1016/j.exer.2008.07.016> (2008).
40. Roberts, M. R., Srinivas, M., Forrest, D., Morreale de Escobar, G. & Reh, T. A. Making the gradient: thyroid hormone regulates cone opsin expression in the developing mouse retina. *Proc Natl Acad Sci USA* **103**, 6218–6223, <https://doi.org/10.1073/pnas.0509981103> (2006).
41. Garcia, T. Y., Gutierrez, M., Reynolds, J. & Lamba, D. A. Modeling the Dynamic AMD-Associated Chronic Oxidative Stress Changes in Human ESC and iPSC-Derived RPE Cells. *Invest Ophthalmol Vis Sci* **56**, 7480–7488, <https://doi.org/10.1167/iovs.15-17251> (2015).
42. FitzSimmons, J., Fantel, A. & Shepard, T. H. Growth parameters in mid-trimester fetal Turner syndrome. *Early human development* **38**, 121–129 (1994).
43. Shepard, T. H. Agents that cause birth defects. *Yonsei medical journal* **36**, 393–396, <https://doi.org/10.3349/ymj.1995.36.5.393> (1995).
44. Numata, S., *et al.* DNA methylation signatures in development and aging of the human prefrontal cortex. *Am J Hum Genet.* Feb 10, **90**(2), 260–72, <https://doi.org/10.1016/j.ajhg.2011.12.020> (2012).
45. Dunning, M. J., Barbosa-Morais, N. L., Lynch, A. G., Tavare, S. & Ritchie, M. E. Statistical issues in the analysis of Illumina data. *BMC Bioinformatics* **9**, 85, <https://doi.org/10.1186/1471-2105-9-85> (2008).
46. Dunning, M. J., Ritchie, M. E., Barbosa-Morais, N. L., Tavare, S. & Lynch, A. G. Spike-in validation of an Illumina-specific variance-stabilizing transformation. *BMC research notes* **1**, 18, <https://doi.org/10.1186/1756-0500-1-18> (2008).
47. Triche, T. J., Weisenberger, D. J., Van Den Berg, D., Laird, P. W. & Siegmund, K. D. Low-level processing of Illumina Infinium DNA Methylation BeadArrays. *Nucleic Acids Research* **41**, e90–e90, <https://doi.org/10.1093/nar/gkt090> (2013).
48. Aryee, M. J. *et al.* Minfi: a flexible and comprehensive Bioconductor package for the analysis of Infinium DNA methylation microarrays. *Bioinformatics*, <https://doi.org/10.1093/bioinformatics/btu049> (2014).
49. Jones, M. J., Goodman, S. J. & Kobor, M. S. DNA methylation and healthy human aging. *Aging Cell* **14**, <https://doi.org/10.1111/accel.12349> (2015).
50. Jung, M. & Pfeifer, G. P. Aging and DNA methylation. *BMC Biology* **13**, 1–8, <https://doi.org/10.1186/s12915-015-0118-4> (2015).
51. Rakyan, V. K. *et al.* Human aging-associated DNA hypermethylation occurs preferentially at bivalent chromatin domains. *Genome Res* **20**, 434–439, <https://doi.org/10.1101/gr.103101.109> (2010).
52. Teschendorff, A. E. *et al.* Age-dependent DNA methylation of genes that are suppressed in stem cells is a hallmark of cancer. *Genome Res* **20**, 440–446, <https://doi.org/10.1101/gr.103606.109> (2010).
53. Teschendorff, A. E., West, J. & Beck, S. Age-associated epigenetic drift: implications, and a case of epigenetic thrift? *Human Molecular Genetics* **22**, R7–R15, <https://doi.org/10.1093/hmg/ddt375> (2013).
54. Bocklandt, S. *et al.* Epigenetic predictor of age. *PLoS One*. **6**, <https://doi.org/10.1371/journal.pone.0014821> (2011).
55. Ohlemacher, S. K., Iglesias, C. L., Sridhar, A., Gamm, D. M. & Meyer, J. S. Generation of highly enriched populations of optic vesicle-like retinal cells from human pluripotent stem cells. *Current protocols in stem cell biology* **32**, 1h.8.1–20, <https://doi.org/10.1002/9780470151808.sc01h08s32> (2015).
56. Phillips, M. J. *et al.* Generation of a rod-specific NRL reporter line in human pluripotent stem cells. *Sci Rep* **8**, 2370, <https://doi.org/10.1038/s41598-018-20813-3> (2018).
57. Meyer, J. S. *et al.* Modeling early retinal development with human embryonic and induced pluripotent stem cells. *Proc Natl Acad Sci USA* **106**, 16698–16703, <https://doi.org/10.1073/pnas.0905245106> (2009).

Acknowledgements

The authors acknowledge the following funding sources for support of this work: NIH NEI grants 1R01EY021482 to T.A.R. and 5F32 EY025117 to A.H., and the Allen Distinguished Investigator awards (Paul G. Allen Family Foundation) to T.A.R. and to S.H. We thank the Vision Core Grant P30EY01730 for the imaging facilities. We thank the Birth Defects Research Laboratory at the University of Washington for making the tissue samples available. We thank the Fred Hutch Genomics Shared Resource for the RNAseq analysis. We thank Alex Chitsazan for data analytics suggestions. Lastly, we thank members of the Reh and Birmingham-McDonogh labs for valuable discussion, and Drs. Olivia Birmingham-McDonogh and R. Wong for constructive comments on the manuscript.

Author Contributions

Akina Hoshino, Steve Horvath, Akshayalakshmi Sridhar and Thomas A. Reh designed and conceived the experiments. Akina Hoshino and Akshayalakshmi Sridhar performed sample preparations, immunohistochemistry, and confocal imaging. RNAseq data was analyzed by Alex Chitazan, Akina Hoshino, Akshayalakshmi Sridhar, Thomas A. Reh and DNA methylation array data was analyzed by Steve Horvath. The manuscript was written and edited by all authors.

Additional Information

Supplementary information accompanies this paper at <https://doi.org/10.1038/s41598-019-39919-3>.

Competing Interests: The authors declare no competing interests.

Publisher's note: Springer Nature remains neutral with regard to jurisdictional claims in published maps and institutional affiliations.



Open Access This article is licensed under a Creative Commons Attribution 4.0 International License, which permits use, sharing, adaptation, distribution and reproduction in any medium or format, as long as you give appropriate credit to the original author(s) and the source, provide a link to the Creative Commons license, and indicate if changes were made. The images or other third party material in this article are included in the article's Creative Commons license, unless indicated otherwise in a credit line to the material. If material is not included in the article's Creative Commons license and your intended use is not permitted by statutory regulation or exceeds the permitted use, you will need to obtain permission directly from the copyright holder. To view a copy of this license, visit <http://creativecommons.org/licenses/by/4.0/>.

© The Author(s) 2019